BIPN 162 Final Project

I. Overview

For this project, we aimed to recreate the topological data analysis pipeline used by Torres-Espín et al. to look at the relationship between intraoperative hemodynamic time series data and spinal cord injury recovery (based on improvement in AIS grade), as well as potential differences in patterning based on patient sex. Our work involved dimensionality reduction, k nearest neighbors clustering, and network analysis. We created simulated data that was biased to reduce chances of AIS grade improvement based on time spent outside the paper's proposed optimal mean arterial pressure range, and we tested our analysis on both the original dataset as well as our own simulated one.

II. Introduction & Background

The spinal cord consists of a bundle of interconnected nerves and nerve fibers that send and receive signals from the brain and the peripheral nervous system. Direct damage that occurs to this network, which begins from the base of the brain and and at the lower back, are defined as spinal cord injury (SCI). Depending on the location and extent of the injury, untreated SCI can cause permanent alterations in feeling and strength, alongside a multitude of bodily functions associated with perception, below the points of where the injury is located (NINDS, 2022).

Previous studies on the demographic distribution of women and men with SCI have yielded notable differences in the age and location of which these injuries occur. For instance, Hu et al.'s 1996 analysis of spinal fracture cases over a 3 year period noted that male patients tended to be injured in their 20s and 30s, while women were more likely to be injured in their 50s and 60s. The study also highlighted SCI injuries were skewed by sex, with male patients presenting approximately 80% of overall cases (Hu et al., 1996). A similar study by Shackelford et al. (1998) further identified location of injury differed between sexes, with female SCI patients more likely to become paraplegics (i.e., lower body paralysis). In contrast, male SCI patients were more likely to become quadriplegics (i.e., whole body paralysis)(Shackelford et al., 1998).

While hospitals around the U.S. were estimated to gain around 18,400 new SCI cases as of 2024 (National Spinal Cord Injury Statistical Center, 2025), unavailability of sex-stratified SCI prevalence and treatment data has persisted into the 2020s. Raguidin et al.'s 2021 review on the gender gap in papers studying cardiometabolic risk and SCI identified only 9 of 15 studies released in the last 3 decades included sex as a collected metric for patient data. No study that included both sexes conducted meaningful sex-specific analyses due to small sample sizes (Raguindin et al., 2021). Given the field's understanding of how age and location of SCI injury differ by sex and the sex-based differences in debilitating health outcomes including paralysis, analyzing patient data by sex could provide vital insight into biological differences between patients that come into play during SCI treatment and recovery.

Torres-Espín et al.'s 2021 paper, *"Topological network analysis of patient similarity for precision*

management of acute blood pressure in spinal cord injury", aimed to improve clinical and research understanding of how neurological recovery following SCI could be predicted. They thus pursued creating a predictive model for postoperative SCI recovery based on various data that examined the relationship between mean arterial pressure (MAP) and subsequent recovery outcomes reported in both human patient and rodent studies over the past decade.

A foundational paper for this study was the 2019 retrospective analysis by Ehsanian et al., which investigated the association between MAP labels recorded during SCI surgery and changes in patients' International Standards for Neurological Classification of Spinal Cord Injury (ISNCSCI) motor score immediately before surgery and following the patients' discharge from rehabilitation. This analysis produced a significant regression equation that indicated patients who maintained MAP levels within a range of 70 and 94 mmHg during surgery experienced greater improvements in motor function following rehabilitation than patients whose intraoperative MAP levels measured outside this range (Ehsanian et al., 2019).

Building on Ehsanian et al.'s 2019 study, Torres-Espín et al. incorporated work from a 2015 study by Nielsen et al. which employed topological data analysis to model the relationship between MAP and functional recovery in SCI using rat models. Using this model, Nielsen et al (2015) similarly found that rats with a within a higher-than-normal, or hypertensive, MAP range were more likely to recover motor function than rats who were outside this range. Using the findings of these papers, Torres-Espín et al. sought to adapt a similar approach using topological data analysis using human clinical data that also could account for the heterogeneity in SCI injuries found in human SCI patients. Ultimately, the goal of their paper was to develop a model that predicted a lower likelihood of neurological recovery in patients if their MAP range during SCI surgery deviated from the optimal range (Torres-Espín et al., 2021).

Torres-Espín et al. utilized both SCI surgical and rehabilitation data from the Zuckerberg San Francisco General Hospital and Santa Clara Valley Medical Center collected between 2003 and 2015 (Torres-Espín et al., 2021). This combined dataset was able to provide a foundation that could assess the relationship between intraoperative MAP and long-term recovery in human patients to corroborate the optimal MAP range associated with favorable function outcomes that was established in previous human SCI rehabilitation studies.

The novel approach this study took to examine this relationship was by applying topological data analysis (TDA) to a human SCI clinical dataset. TDA is a method that is often used for finding patterns in complex and high-dimensional data by allowing researchers to maintain the shape of the data but identify clusters of non-linearly-related characteristics within the dataset that might have been obscured if using an analysis method that solely focused on linear relationships (Frédéric & Michel, 2017). For this study, TDA was used to identify patient subgroups with similar physiological profiles in heart rate (HR) and MAP while also exploring how these similarities related to functional recovery outcomes. The use of TDA thus resolves the issue Torres-Espín et al was concerned with regarding heterogeneous human clinical data, as

variations in patient data would be now adequately captured.

To build their prediction model, Torres-Espín et al used the 2 patient datasets to assess similarities in MAP and HR values recorded between patients and apply dimensionality reduction using an Isomap algorithm. These analyses ultimately were used to perform a topological network analysis that visualized patient connectivity based on the MAP and HR values. A regression analysis was then conducted to model the probability of neurological functional improvement using MAP measurements. The final predictive model employed used 3 binary outcome metrics: whether patients improved by at least one grade on the AIS improvement of at least one grade on the American Spinal Injury Association Impairment scale (AIS) from admission to discharge, whether patients were classified as the higher AIS grade (A) at discharge, and whether the patients were classified as the lowest AIS grade (D) at discharge (Torres-Espín et al., 2021).

In an effort to consider how non-physiological patient characteristics like sex influence recovery prediction, we sought to further test this model by stratifying a subset of patients by sex using a simulated dataset. While we attempted to use a different dataset that incorporated a subset of patients also used in the Santa Clara Valley Medical Center file that detailed more demographic characteristics from the original dataset like sex, we were unable to appropriately match the sex of patients from the smaller dataset to the larger one used in Torres-Espín et al. (2021). This stratification will allow for a closer examination of whether recovery patterns in SCI patients have a sex-specific correlation that could be detected by the predictive model. The simulated dataset also included sex as a variable to allow use to evaluate whether the model could consistently predict patient recovery outcomes across various conditions within patient profiles.

III. Replication

For us to use the TDA pipeline Torres-Espín et al had created, we first needed to convert the cells we needed from the original pipeline from its originally-written R into python. To ensure that this pipeline was still able to accurately reproduce the statistics it generated in the original pipeline, we then ran the patient data taken from electronic health records at the Zuckerberg San Francisco General Hospital and Santa Clara Valley Medical Center.

To preprocess the raw patient data, Torres-Espín et al. (2021) first isolated patients with high-frequency intraoperative physiological data as the higher resolution of MAP signals would allow for more accurate grouping during TDA. This data was further filtered to remove values in MAP recordings that were not plausible for human patients to make (i.e., this threshold was set to any 80 mmHg < MAP < 20 mmHg). Additionally, MAP data was segmenting into 10 minute intervals to calculate measures of central tendency like mean and standard deviation, skew, and quantile characteristics. This processed data was then reincorporated with demographic characteristics like age and physiological characteristics like heart rate trends into the ODC files we used to recreate the TDA pipeline in python. The final dataset consists of 118 patients from both hospitals.

The original dataset with MAP and HR time series from the paper was available as 2 csv files for

2 sets of patients. Rows represented individual patients; the first half of the columns were for HR time series data in 5 minute intervals and the second half of the columns were for MAP time series data in 5 minute intervals. We combined the 2 sets of patients into one larger pandas dataframe, which was then split into two dataframes based on whether they were MAP or HR values.

The data analysis pipeline we have derived from the TDA analysis pipeline created by Torres-Espín et al. (2021) compares MAP and HR data from SCI patients but is condensed to visualize the specific graphs we hoped to generate. First, the processed patient dataset is separated into 2 csv files, with one containing only MAP data and the other containing only HR data. Each patient's data is then transformed using an empirical cumulative distribution function (ECDF) to convert the trends in MAP and HR data to place less emphasis on the magnitude of the values and emphasize the shapes or patterns found in the data. Then, a pairwise Euclidean distance matrix is conducted between patients using the feature vectors from the ECDF to determine how similar each patient's MAP-HR profile was to others in the dataset.

The ECDF matrix is then reduced in dimensionality using Isomap after selection for values of k, the number of neighbors, and d, the number of dimensions preserved. The values of k and d are selected based on how well they preserve the residual variance and minimize zero-dimensional and one-dimensional Wasserstein distances. A mutual k-nearest neighbor graph is constructed in the embedded lower dimensional space, with the minimum k selected to ensure the graph is fully connected. The resulting graph is analyzed using the Walktrap algorithm, which detects clusters of patients based on short random walks. The optimal number of steps for Walktrap is chosen by maximizing modularity.

Topological data analysis (TDA) is then performed using *Ripser* and *Persim* packages. *Ripser*, which computes persistent homology, is performed on the ECDF-transformed vectors to identify topological features within the data. *Persim* is then used to visualize the persistence diagrams that describe how the relationships between the feature vectors are affected as the threshold parameter increases and ultimately identify higher-order, nonlinear patterns. Following TDA, a k-nearest neighbor (k-NN) graph is constructed using input from the ECDF vectors. A k-nearest neighbors classifier is trained using the ECDF features. When the simulated dataset is incorporated, accuracy is also calculated to evaluate how well the transformed data distinguishes between the real and simulated patient groups.

The figures shown below compares the impacts of different k values (near neighbor values) and d values (number of dimensions preserved) on distance preservation and topological persistent homology preservation. The first row is figures from the original paper, while our generated figures are in the second row. The residual variance is calculated for the geodesic distance matrix for each k value and the Euclidean distance matrix of the low-dimensional solution. The next two graphs are for the zero-dimensional and one-dimensional Wasserstein distances. Although our pipeline's residual values were the same

as the ones from the paper, our values for the Wasserstein distances did not match. The trend was similar for the zero-dimensional distance, but not very similar for the one-dimensional distance. This may be due to differences in the filtration used by *Persim*, the package we used for the Wasserstein calculation, and the one used in the original paper.

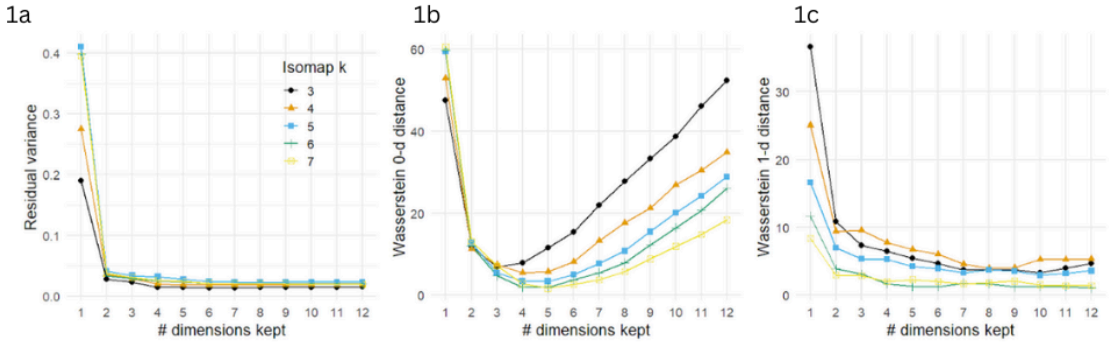

Fig 1A-C: Graphs depicting Residual Variance, Wasserstein 0D distance, and Wasserstein 1D distance within the original dataset. Taken from the paper.

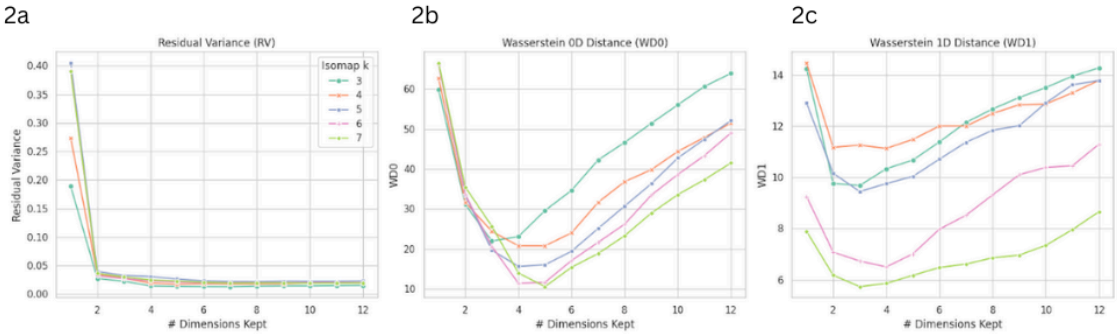

Fig 2A-C: Graphs depicting Residual Variance, Wasserstein 0D distance, and Wasserstein 1D distance within the original dataset. Generated by us.

The figures below the network clustering results, where blue is the image from the paper and red is our recreation. Each node represents a patient. This visualization of the similarity of patients in the low-dimensional space is constructed after dimensionality reduction via Isomap based on k = 6 and d = 4. Then, a k nearest neighbor graph is applied to find edges between nodes. Although there are some differences in presentation and flattening, they have extremely similar patterns and clustering.

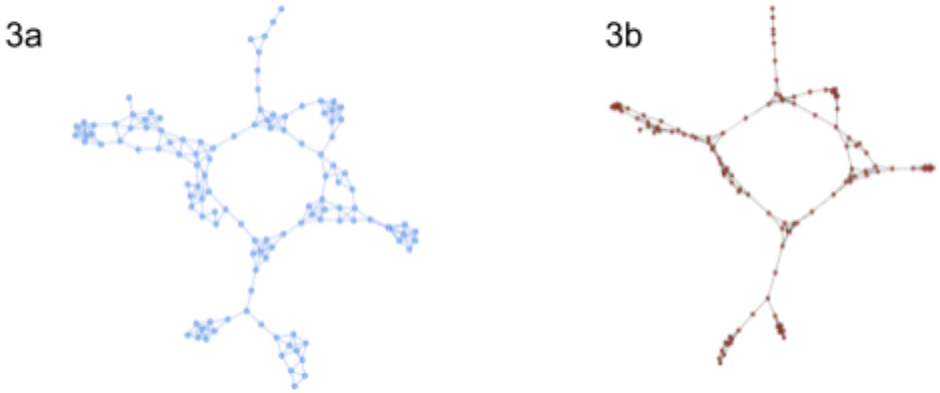

Fig 3A and B: Comparison of Topological Data Analysis between the original dataset (3A) and the simulated dataset (3B)

The figures below show the mapping of average MAP values on the similarity and cluster networks. The patterns in clustering for MAP values. Although our graph is oriented and flattened differently, they show similar clustering patterns. Additionally, the box and whisker plots for average MAP are ordered differently, but they exhibit extremely similar patterns by color. This suggests that our data analysis found similar clustering patterns to the original paper.

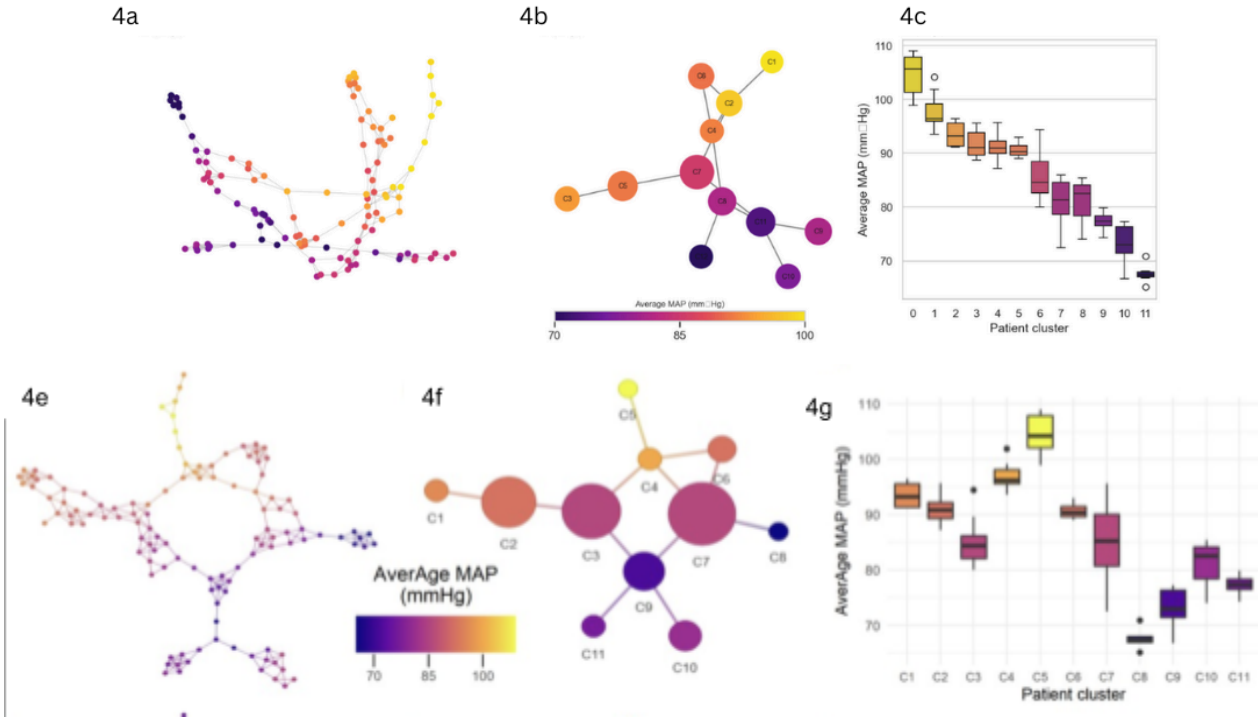

Fig 4A-C: Graphs depicting 2D manifold embedding of patient aMAP data using Isomap (4A), Node graph depicting relationships with clusters (4B), and a boxplot of aMAP values group by cluster (4C) using the original dataset. Generated by us.
Fig 4E-G: Graphs depicting 2D manifold embedding of patient aMAP data using Isomap (4A),

Node graph depicting relationships with clusters (4B), and a boxplot of aMAP values group by cluster (4C) using the original dataset. From the original paper.

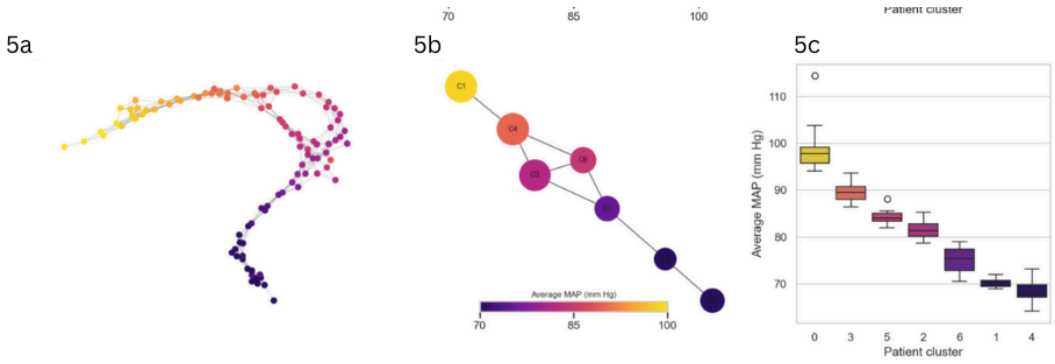

Fig 5A-C: Graphs depicting 2D manifold embedding of patient data using Isomap (5A), Node graph depicting relationships with clusters (5B), and a boxplot of MAP values group by cluster (5C) using the simulated dataset

IV. Additional dataset Analysis & Results

To construct our pipeline, we were able to use the same processed dataset Torres-Espín et al. used to generate their original TDA pipeline. The patient data used in this project was taken from electronic health records at the Zuckerberg San Francisco General Hospital and Santa Clara Valley Medical Center. These files were downloaded from the Open Data Commons for Spinal Cord Injury (ODC-SCI), and were preprocessed prior to their upload to the data sharing platform. While we wanted to test the robustness of our pipeline through a SCI patient dataset collected from a different hospital in the United States, there was no open-access data available on ODC-SCI or any other database that provided the sex of the patient, trends in MAP, and was compatible with our pipeline. We thus opted to use a simulated dataset of a hypothetical patient population using our original dataset as a guide.

Data was generated for 100 patients with random ages (between 18 and 85 years) and sex (60% male, 40% female). AIS grade at admission was sampled from a categorical distribution over values 1-5 (representing AIS grades A-E) with probabilities [0.40, 0.15, 0.15, 0.24, 0.06]. Surgery durations were selected from a uniform distribution between 120 and 900 minutes. A time series for each patient was generated, where the surgery duration was split into 5 minute intervals and MAP values were generated at each interval. A starting MAP value for each patient was generated using a normal distribution centered at 85 mmHg and a standard deviation of 5 mmHg. A time series for MAP values was generated by using a random walk process with Gaussian noise centered at 0 with a standard deviation of 2 mmHg. To make it somewhat more realistic and avoid large proportions of a series being outside the optimal range, values were softly reflected at upper and lower bounds of 55 and 130 mmHg.

For each patient, the proportion of MAP readings outside the optimal range (76–104 mmHg, based on the paper) was calculated. A logistic regression model was used to convert this proportion into a probability of AIS improvement, using the equation logit(p)=0.35-2.0*(proportion

of time out of range). Binary AIS improvement (0 = no improvement, 1 = improved) was simulated using a Bernoulli trial with the computed probability. Discharge AIS grades were set to admission grade plus one if improved, capped at a maximum grade of 5.

The resulting dataset includes two CSV files: simulated_patients.csv, containing summary-level patient data (demographics, AIS grades, MAP deviation, outcomes), and simulated_map_timeseries.csv, containing the full intraoperative MAP time series for each patient across 5-minute intervals. The simulated_map_timeseries.csv file was further separated into one file specifically containing data for the 40 simulated female patients, and another file specifically containing data for 60 simulated male patients.

The dataset we generated is biased to have a relationship between the proportion of time the patient spends outside the optimal MAP range and the probability of an improvement in their AIS grade, and more time outside the range reduces the probability of AIS improvement. This allows us to test the model established in the paper, which is limited to data from two hospitals in the Bay Area, on data with a known relationship. In other words, the model should show similar patterns of a correlation between time spent in the optimal range and AIS improvement for our data. This allows us to address two questions. First, are the paper's findings valid outside of their dataset, which is limited to a concentrated geographic area that could have skewed population demographics? Secondly, can our pipeline accurately analyze datasets where sample sizes are less than 100, of which could arise from studying smaller male-specific and female-specific SCI patient populations?

Since we generated the data ourselves using a preprocessed dataset, we did not have to take additional steps to organize it into a specific format. During data generation, the simulated intraoperative MAP values for each patient with an interval of 5 minutes was organized into a pandas dataframe of size number of patients by the max number of intervals+1. The first column had patient IDs and the remaining columns were time intervals of 5 minutes. Each row had time series data for one patient.

To ensure that our code ran as expected, we placed several checkpoints. The first checkpoint was within the ECDF Matrix, in which all entries were converted to numeric types and any errors to NaN, which helped identify erroneous or missing data in the dataset earlier in the notebook. The first few rows of the ECDF Matrix were also visualized using the .head() pandas method to show that the values were structured correctly and that the transformation had succeeded. Additionally, we were able to use qualitative validation for all of the plots and diagrams we generated by comparing them against those generated by the original dataset provided by Torres-Espín et al. This was especially useful in creating the isomaps as we were able to visually confirm that clusterings of patient data by feature vectors did occur.

The main way we know our iterative procedure used in our notebook converged is by

looking at the output given by the cells in which Isomap was conducted. While we did not explicitly test for convergence, when our cells were run, no errors were raised in the notebook and a print of the data used in the Isomap did not show any presence of NaN values. The error free dataset used in the Isomap and the visualization of the patient clusters indicates the Isomap was able to converge successfully and produce meaningful results.

The following visual containing figures 6A through 6F represented the residual variance, wasserstein 0D distance, and wasserstein 1D distance. The same plots created using the original dataset (1A-C) were also included for ease of comparison.

Similar to the results obtained in the original dataset, most of the structure of the male and female specific simulated data is captured within the first 3-4 dimensions and the pattern is consistent along the different k values. The flattening of the residual variance trends as dimensions increase further indicate convergence of the data, as there is little difference in variance reduction. The results of the wasserstein 0D are also similar across datasets. The wasserstein 1D visualize a difference between the sex-specific simulated (6C and 6F) and original dataset (1c) in that while 1C has a sharper drop in trend as more dimensions are kept, 6C and 6F see a rise after 3 dimensions.

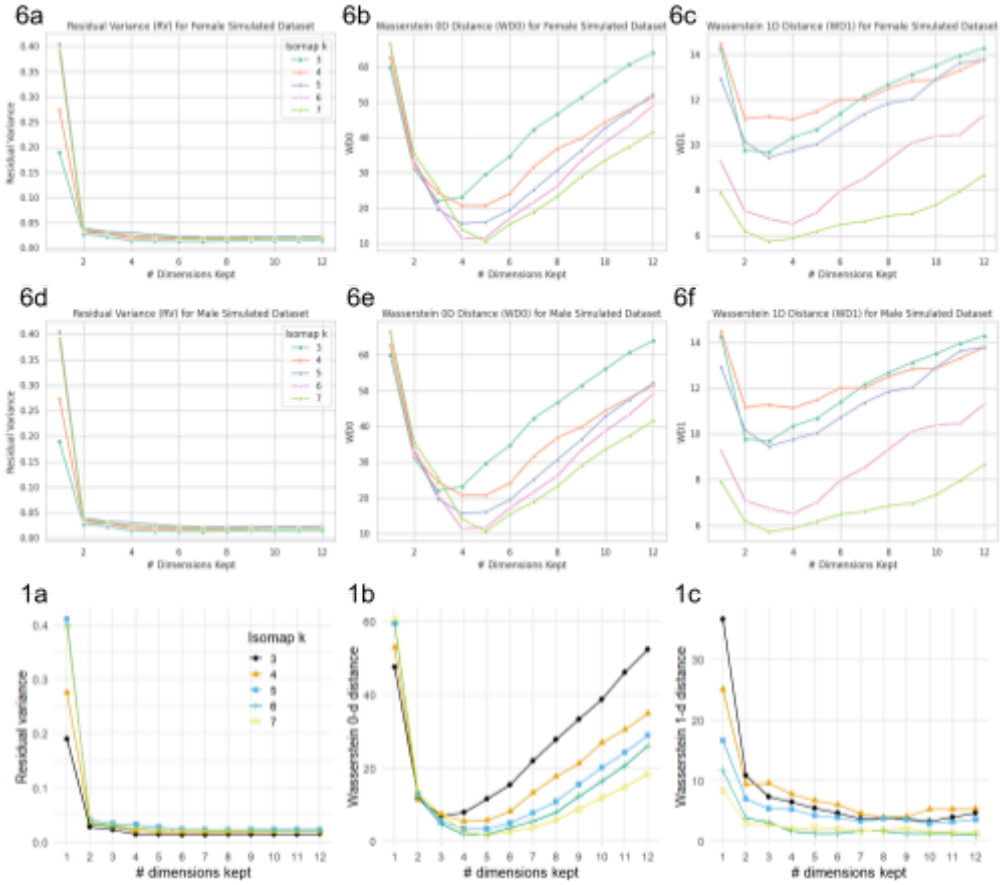

Fig 6A-F: Graphs depicting Residual Variance (6A), Wasserstein 0D distance (6B), and Wasserstein 1D distance (6C) within the simulated Female-specific simulated dataset and Residual Variance (6D), Wasserstein 0D distance (6E), and Wasserstein 1D distance (6F) within the simulated Male Specific simulated dataset

The network visualization of the male and female specific datasets shows interesting differences between sexes. structure collapses into a sparse, tree-like backbone with few redundant triangles or 4-cliques; most nodes sit on a single primary branch and side-branches are short, implying that female patients occupy a narrower, more linear spectrum of physiologic states. The male-only network (panel 8b) shows the opposite pattern: the graph stretches into an elongated ribbon reinforced by numerous overlapping triangles, so connectivity is evenly distributed along the arc rather than focused in a hub.

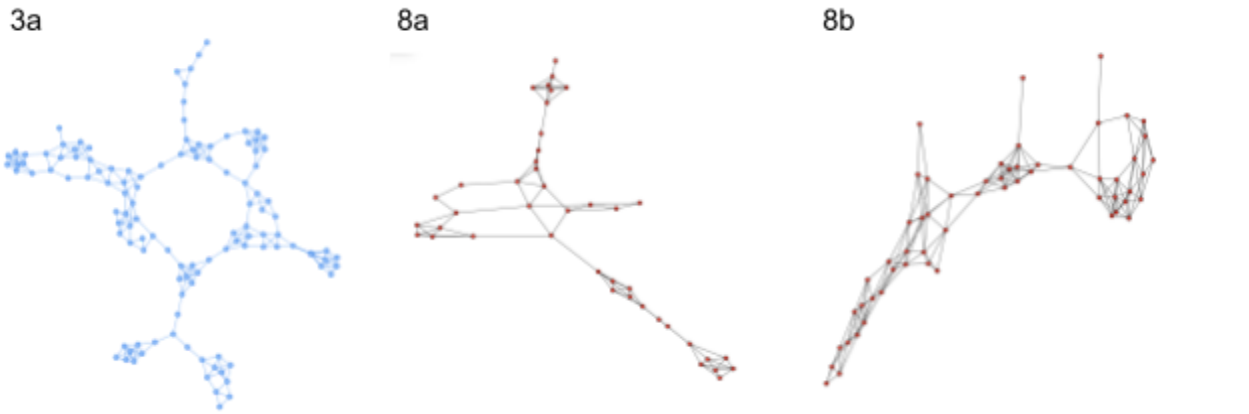

Fig 8A and B: Comparison of Topological Data Analysis between the Female-specific simulated dataset (8A) and the Male-specific simulated dataset (8B)

In the female Isomap embedding (9A) patients lie on a gently curved spine whose colour gradient runs smoothly from purple (low MAP) through orange to yellow (high MAP). Clustering collapses this arc into five clusters (9B): two high-MAP “end-caps” (C1, C5), a mid-MAP core (C3), and two low-MAP groups (C2, C4). The box-plot (9C) shows a near-monotonic descent in average MAP from C3 ≈ 95 mm Hg down to C2/C4 ≈ 70–75 mm Hg. The narrow inter-quartile ranges indicate that female clusters are internally homogeneous. The male manifold (9D) looks markedly different: the embedding wraps into an elongated ‘S’ with sharper bends and far denser local connectivity. Walktrap merges the ribbon into four clusters (9E) that sit sequentially along the path, but the distances between nodes are larger and the mid-MAP segment (C2) is much thinner than in females. Consequently, the male box-plot (9F) reveals a wider MAP spread within each cluster (especially C3 and C1) and a steeper overall gradient, from ~102 mm Hg in C0 down to ~65 mm Hg in C1. Overall the comparison reinforces the earlier topological observation: females occupy a narrow, smoothly varying MAP continuum that can be partitioned into compact, almost one-dimensional communities, whereas males populate a broader, more tortuous manifold whose clusters retain greater internal variability. These distinctions suggest that sex-specific thresholds may be required when using MAP to stratify risk or predict neurologic outcomes.

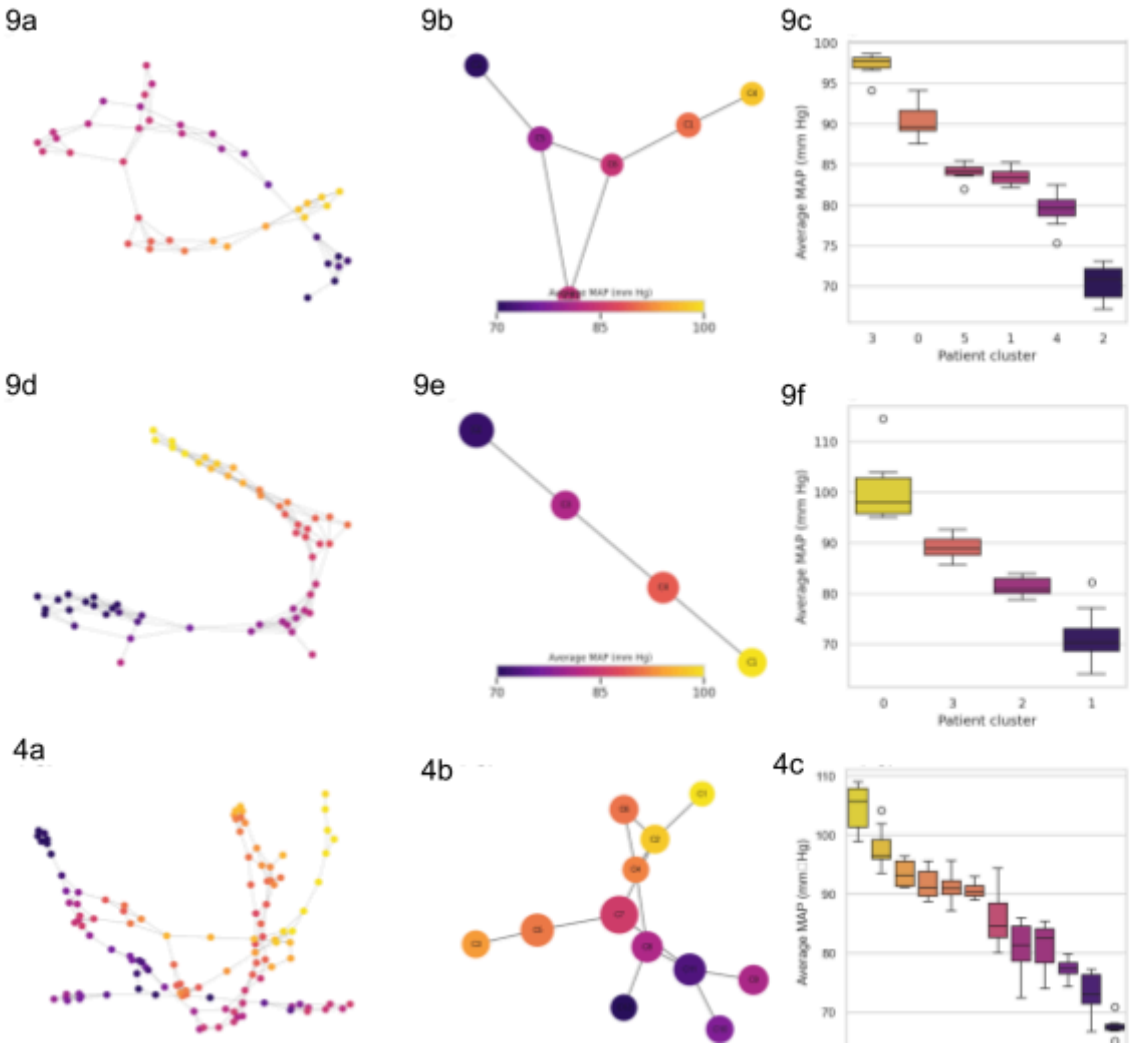

Fig 9A-F: Graphs depicting female-specific simulated data 2D manifold embedding using Isomap (9A), Node graph depicting relationships with clusters (9B), and a boxplot of MAP values group by cluster (9C) and 2D manifold embedding of male-specific simulated data using Isomap (9D), Node graph depicting relationships with clusters (9E), and a boxplot of MAP values group by cluster (9F)

V. Discussion

Overall, we were able to get the results we expected from the pipeline in the sense that all analyses were successfully translated from R to python and the pipeline was able to handle smaller datasets than the originally-tested dataset of n=118 to create similar graphs to the original dataset. The method performed well relative to the expected results, although there could be further improvements made to reducing the noise in datasets prior to generating the wasserstein 1D plot. This noise could have also been due to the fact that our sex-specific datasets were randomly generated and would not necessarily follow the same distribution as patient data organically gathered in a hospital setting. We were able to capture relationships between patients based on their MAP scores, and we were able to see how patterns may look

very different based on sex. Ideally, we would want to conduct further data analysis and see how the clustering patterns for AIS improvement and MAP scores align to better understand the relationship between sex, MAP patterns, and surgery outcome improvement.

One major consideration is that our findings are inherently limited by the use of a simulated dataset, which uses a simple random walk algorithm to generate a time series of MAP values. This does not capture the real reasons behind and variations of intraoperative MAP data. It is therefore difficult to say whether our data really tests the validity of the model, and ideally we would have liked to test on a real dataset. While we were unable to test our pipeline using a dataset curated by a hospital with a different geographic location and patient population to Torres-Espín et al.'s 2021, the absence of SCI patient data in spite of its rising prevalence in the United States has highlighted a gap in data collection hospitals throughout the United States could seek to fill. Increasing the sample size of patients and their related demographic characteristics could not only improve the robustness of the statistical analysis of the pipeline by using organic data but also improve the generalizability of the pipeline as a prognosis tool for researchers and clinicians to use when considering SCI surgery as a form of treatment.

Initially, we were also confident about our ability to adapt the original code from R to python, but ultimately the process was complicated by the differences in modules and libraries between the two languages. Graphs generated on python also looked different from those on R due to differences in the way packages processed and represented the same dataset. However, this preliminary migration of the pipeline to a more accessible programming language could increase the likelihood of other researchers coming across the pipeline and contributing to the pipeline's improvement.

VI. Feedback Rebuttal

The main feedback we received was about including greater detail in our description of the data analysis method and making sure we had ways to demonstrate whether our model worked. As we moved through the actual coding, we were able to have a better understanding of the data analysis process. This allowed us to write a description of our process in our replication section that is hopefully more detailed. To demonstrate our successful implementation of the method, we used different approaches. To improve upon our initial explanation of TDA and how it is applied, we added a section in our introduction thoroughly explaining the method with a paragraph dedicated to the importance of TDA to the pipeline. We also tried to show our confidence in the code through comparisons between the original plots generated by the paper and the plots generated by the python pipeline we created in the replication section of this paper at various points in the pipeline. We compared a lot of aspects visually since that was a key assessment of the network analysis, but we supplemented this with graphs of information related to different steps. For example, we compared our results for Isomap optimization to the original paper by making graphs of relevant values (residual variance and Wasserstein distances) to compare trends and numbers between our results and the original paper.

VII. Contributions and Signature of Academic Honesty

Aadhya:

- Wrote the code we used to generate the simulated data used for our data analysis.
- Worked on the ECDF, Isomap optimization, and Network clustering portions of the TDA pipeline.

Leanne:

- Conducted literature search for the purpose of our paper
- Worked on translating the original pipeline from R to python. ChatGPT was used to troubleshoot errors that arose from migrating cells from R to Python
- Worked on stratifying the simulated dataset by sex and stratifying the original dataset by MAP and HR and generated graphs for the results section.

Pavan:

- Worked on translating the R code to python to generate the graphs in the project
- Worked on the Network clustering portions of the TDA pipeline. Chatgpt was used to troubleshoot errors and help debug.
- Helped analyze the graphs and note observations in the final write up
-

ChatGPT was used for suggestions for ways to generate data, help with adding comments, as well as small changes to the code for generating the MAP time series. It was also used to help understand some of the original code in R and for suggestions on implementing similar pathways in python.

“The work herein is original and my own and my claims are truthful as far as I understand. I checked all generative AI results that I used for truthfulness and I can explain every line of code that we used.”

Aadhya Tripathi, Leanne Liaw, Pavan Punnamraju

VIII. References

Ehsanian, R., Haefeli, J., Quach, N., Kosarchuk, J., Torres, D., Stuck, E. D., Endo, J., Crew, J. D., Dirlikov, B., Bresnahan, J. C., Beattie, M. S., Ferguson, A. R., & McKenna, S. L. (2019). Exploration of surgical blood pressure management and expected motor recovery in individuals with traumatic spinal cord injury. *Spinal Cord*. https://doi.org/10.1038/s41393-019-0370-5

Frédéric , C., & Michel, B. (2017). An introduction to Topological Data Analysis: fundamental and practical aspects for data scientists. *ArXiv (Cornell University)*. https://doi.org/10.48550/arxiv.1710.04019

Hu, R., Mustard, C. A., & Burns, C. (1996). Epidemiology of Incident Spinal Fracture in a Complete Population. *Spine*, *21*(4), 492–499. https://doi.org/10.1097/00007632-199602150-00016

National Spinal Cord Injury Statistical Center. (2025). *Traumatic Spinal Cord Injury Facts and Figures at a Glance 2025 SCI Data Sheet*. University of Alabama at Birmingham. https://bpb-us-w2.wpmucdn.com/sites.uab.edu/dist/f/392/files/2025/02/2025-Facts-and-Figures.pdf

Nielson, J. L., Paquette, J., Liu, A. W., Guandique, C. F., Tovar, C. A., Inoue, T., Irvine, K.-A., Gensel, J. C., Kloke, J., Petrossian, T. C., Lum, P. Y., Carlsson, G. E., Manley, G. T., Young, W., Beattie, M. S., Bresnahan, J. C., & Ferguson, A. R. (2015). Topological data analysis for discovery in preclinical spinal cord injury and traumatic brain injury. *Nature Communications*, *6*(1), 8581. https://doi.org/10.1038/ncomms9581

NINDS. (2022). *Spinal cord injury*. Www.ninds.nih.gov; National Institute of Neurological Disorders and Stroke. https://www.ninds.nih.gov/health-information/disorders/spinal-cord-injury

Raguindin, P. F., Muka, T., & Glisic, M. (2021). Sex and gender gap in spinal cord injury research: Focus on cardiometabolic diseases. A mini review. *Maturitas*, *147*, 14–18. https://doi.org/10.1016/j.maturitas.2021.03.004

Shackelford, M., Farley, T., & Vines, C. L. (1998). A comparison of women and men with spinal cord injury. *Spinal Cord*, *36*(5), 337–339. https://doi.org/10.1038/sj.sc.3100510

Torres-Espín, A., Haefeli, J., Ehsanian, R., Torres, D., Almeida, C. A., Huie, J. R., Chou, A., Morozov, D., Sanderson, N., Dirlikov, B., Suen, C. G., Nielson, J. L., Kyritsis, N., Hemmerle, D. D., Talbott, J. F., Manley, G. T., Dhall, S. S., Whetstone, W. D., Bresnahan, J. C., & Beattie, M. S. (2021). Topological network analysis of patient similarity for precision management of acute blood pressure in spinal cord injury. *ELife*, *10*, e68015. https://doi.org/10.7554/eLife.68015